Tunable Bandgap in Bilayer Armchair Graphene Nanoribbons: Concurrent Influence of Electric Field and Uniaxial Strain

Kaveh Khaliji, Maziar Noei, Seyed Mohammad Tabatabaei, Mahdi Pourfath, *Member, IEEE*, Morteza Fathipour, *Member, IEEE*, and Yaser Abdi

***Abstract*— In this paper, the effect of uniaxial strain on the electronic properties of bilayer armchair graphene nanoribbons (BLAGNRs) is theoretically investigated for the first time. Our calculations based on density functional theory (DFT) reveal the tunable nature of the electronic properties of BLAGNRs with the application of uniaxial strain. We further explore the simultaneous effect of perpendicular electric field and uniaxial strain on the electronic bandgap. The results show that as long as the strain induced bandgap is smaller than a critical value of 0.2 eV, the electric field can significantly modulate the bandgap. In addition, we modified nearest neighbor tight-binding (TB) parameters to include the effect of the hydrogen passivation, which results in an excellent agreement between the electronic bandstructures obtained from DFT and TB calculations. Finally, by employing the nonequilibrium Green's function formalism, an on-off conductance ratio as high as 10^5 is predicted for strained BLAGNRs.**

***Index Terms*— Ballistic transport, bilayer graphene nanoribbons, density functional theory, electric field effect, uniaxial strain.**

I. Introduction

THE ADVENT of graphene, a carbon-based material of atomic thickness with high carrier mobility, marks a milestone in the research on 2-D nanostructures [1]. However, the semimetal nature of graphene acts as a serious obstacle for its use in digital logic applications. To overcome this issue, three methods have been developed so far: applying a vertical electric field to bilayer graphene (BLG) [2]–[4]; confining the charge carriers in graphene sheets known as graphene nanoribbons (GNRs) [5]–[10]; and exerting strain on graphene [11]–[13].

Manuscript received March 3, 2013; revised May 3, 2013; accepted May 28, 2013. Date of publication June 17, 2013; date of current version July 19, 2013. This work, as part of the European Science Foundation's EUROCORES program EuroGRAPHENE, was supported by the Austrian Science Fund under Contract I420–N16. The review of this paper was arranged by Editor J. Knoch.

K. Khaliji, M. Noei, S. M. Tabatabaei, and M. Fathipour are with the Department of Electrical and Computer Engineering, University of Tehran, Tehran 14395-515, Iran (e-mail: kavehkhaliji@ut.ac.ir; maziar.noei@gmail.com; smtsbu@gmail.com; mfathi@ut.ac.ir).

M. Pourfath is with the Department of Electrical and Computer Engineering, University of Tehran, Tehran 14395-515, Iran and also with the Institute for Microelectronics, Technische Universität Wien, Gusshaustrasse 27-29/E360, 1040 Wien, Austria (e-mail: pourfath@iue.tuwien.ac.at).

Y. Abdi is with the Department of Physics, University of Tehran, Tehran 145888-9694, Iran (e-mail: y.abdi@ut.ac.ir).

Color versions of one or more of the figures in this paper are available online at http://ieeexplore.ieee.org.

Digital Object Identifier 10.1109/TED.2013.2266300

As predicted by the International Technology Roadmap for Semiconductors [14], at 12-nm technology node where silicon-based field effect transistors (FETs) reach their physical limits due to adverse short channel effects [15], for grapheme-based FETs to be an ideal alternate, an energy gap of at least 0.4 eV is required. Both theoretical [16], [17], and experimental [3] investigations show that in BLG under vertical electric fields, the maximum achievable energy gap is 0.25 eV, which clearly does not fulfill the desired switching characteristics for digital applications [18]. In addition, although the application of strain causes a relative shift in Dirac cones [12], [13], for opening an energy gap in uniaxially strained graphene one requires deformations as large as 20%, which are impractical [11]. Hence, among the three aforementioned methods, patterning graphene into GNRs, which is realizable by a variety of methods such as chemical synthesizing [7], lithographical patterning [5], [6], and unzipping carbon nanotubes, [8], [10], [19] is the best way to engineer the desired bandgap.

Despite smaller energy gaps in bilayer GNRs (BLGNRs) in comparison with their single layer counterparts (SLGNRs) [20], the fact that BLGNR systems have lower sensitivity to low frequency noise [21], accompanied by a unique property of tunable bandgap with perpendicularly applied electric field [20], render them as more desirable candidates for nanoelectronic applications.

The influence of uniaxial strain on transport properties of SLGNRs is theoretically explored before using tight-binding (TB) model [22] and density functional theory (DFT) calculations [23], [24]. These studies reveal that the electronic properties of armchair SLGNRs (SLAGNRs) can be considerably tuned by the application of external strain. The application of this method to armchair BLGNRs (BLAGNRs) adds another degree of freedom to the available routes for manipulating the bandgap in BLGNRs.

In this paper as the first step, TB parameters that include the effect of hydrogen passivation are extracted from DFT calculations. In the next step, the effect of uniaxial strain in the presence of a vertical electric field on the energy bandgap and transport properties of hydrogen passivated BLAGNRs is studied. This paper is organized as follows. After a brief introduction in Section I, the models and numerical methods are explained in Section II. The results for H-passivated BLAGNRs are presented and discussed in Section III. A short summary and concluding remarks are presented in Section IV.

II. Approach

A. DFT Calculations

In this paper, the Vienna *ab initio* simulation package [25], [26] is employed to perform the DFT calculations using the projector augmented wave formalism [27]. For the exchange-correlation potential, the Perdew-Burke-Ernzerhof modification of the local density approximation is utilized [28]. A cutoff energy equal to 500 eV is adopted. A large interlayer spacing of 30 Å is used to assure the elimination of interlayer interactions that are absent in a realistic structure. A 2-D Γ-centered Monkhorstâ€"Pack Brillouin-zone grid of $11 \times 11 \times 1$ k points is chosen for all relaxations. In addition, a convergence criteria of about 10^{-6} eV is considered in all calculations.

B. Tight-Binding Model

The TB Hamiltonian in the second quantized representation for a BLAGNR can be written as follows:

$$\begin{aligned} H = &\sum_{i,m} \mathcal{E}_{on} a^{\dagger}_{m,i} a_{m,i} - \gamma_0 \sum_{\langle i,j\rangle,m} (a^{\dagger}_{m,i} b_{m,j} + H.c) \\ &-\gamma_1 \sum_{i} (a^{\dagger}_{1,i} b_{2,i} + H.c) - \gamma_2 \sum_{i,j} (a^{\dagger}_{1,i} a_{2,j} + H.c) \\ &-\gamma_3 \sum_{i,j} (b^{\dagger}_{1,i} b_{2,j} + H.c) + \frac{\mathrm{q}Ed}{3} \sum_{i} (a^{\dagger}_{2,i} a_{2,i} + b^{\dagger}_{2,i} b_{2,i}) \end{aligned} \tag{1}$$

where $a_{m,i}(b^{\dagger}_{m,i})$ creates (annihilates) an electron in the p_z-orbital centered on i-th carbon atom on sublattice A (B) in plane $m = 1, 2$. In Fig. 1(b), different carbon–carbon interactions that are incorporated into our TB model are shown. γ_0 represents the interaction between the A and B atoms in the x-y plane and is equal to 2.598 eV. $\mathcal{E}_{\mathrm{ON}}$ is the on-site energy for the A atoms in both planes and is equal to –0.026 eV. γ_1 represents the interaction between the A atoms in the lower plane and B atoms in the upper plane that sit exactly above each other and is equal to 0.364 eV. Finally, the interactions between the nearest neighbor A atoms in different planes (γ_2) is equal to 0.319 eV and the corresponding hopping between B atoms (γ_3) is 0.177 eV [29]. The last term in (1) represents the modification of the on-site energies in BLAGNR with interlayer distance d due to an applied vertical electric field, E. Additionally, the screening effect present in the bilayer structure is modeled by reducing the vertical electric field to one-third [30].

To study the effect of strain, the framework of the elasticity theory is utilized in which the atomic positions before and after applying a uniform uniaxial strain along the x-direction can be described by the following relation:

$$\mathbf{R}' = \begin{pmatrix} 1+\sigma & 0 & 0 \\ 0 & 1-\nu\sigma & 0 \\ 0 & 0 & 1 \end{pmatrix} \mathbf{R} \tag{2}$$

where $\mathbf{R}'$ and $\mathbf{R}$ are the deformed and undeformed coordinates, respectively. σ denotes uniaxial strain defined as the change in length per unit length and varies in the range of ±6%. ν represents the PoissonâĿs ratio, relating the subsequent shrinkage in the direction perpendicular to the pulling axis and stretching in the direction perpendicular to the compressing axis.

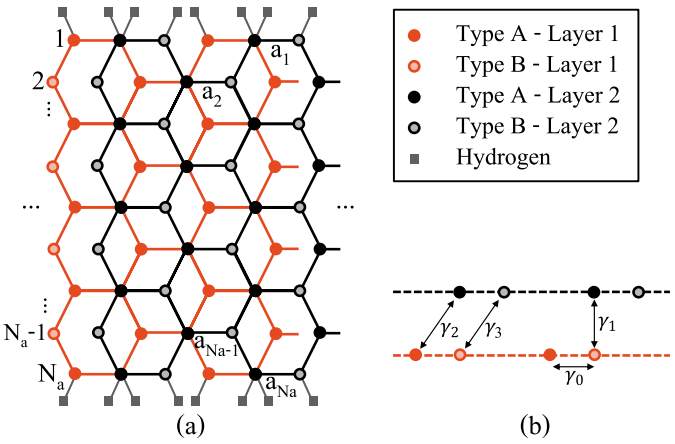

Fig. 1. (a) Top and (b) side view of the structure of an α-aligned N_a-BLAGNR. The C–C bonding length on the nth dimer line is denoted by a_n. The γ_i's represent various C–C hopping parameters.

Upon applying strain to the ribbon, the relative positions of atoms in a unit cell are modified. Hence, the hopping parameters are modulated due to their strong dependence on bonding length. The model described in [31] was adopted in this paper to describe the modulation of the hopping parameters with the bonding length

$$\gamma_i(l) = (l_0/l)^2 \gamma_i(l_0) \left[\frac{1}{1+\exp(46(l/l_0-1))} + \frac{(l/l_0)^{4.3}\exp(4.3(1-l/l_0))}{1+\exp(46(l/l_0-1))} \right] \tag{3}$$

where l_0 and l are the undeformed and deformed bonding length, respectively. This model gives more accurate results than the Harrison's model in describing the interatomic distance dependency of hopping parameters in bi- and multilayer structures [32].

C. Nonequilibrium Green's Function Formalism

The nonequilibrium Green's function (NEGF) formalism is widely used to study nanoscale devices [33]. To evaluate the quantum conductance of the nanoribbons under study, we assume them as channels connecting to two semiinfinite (left and right) leads. Therefore, the retarded Green's function of the channel can be obtained as follows:

$$G_{\mathrm{ch}} = [(E + i\eta)I - H_{\mathrm{ch}} - \Sigma_{\mathrm{L}} - \Sigma_{\mathrm{R}}]^{-1} \tag{4}$$

where η is an infinitesimally small quantity, H_{ch} is the Hamiltonian of the device, and Σ_{R} and Σ_{L} are the the self-energies associated with the right and left contacts, respectively. As mentioned previously, the TB method is utilized to construct the Hamiltonian. Contact self-energies describe broadening and shift of eigenenergies as a result of coupling between the channel and contacts and are given by the following:

$$\Sigma_{\mathrm{L}} = \beta^{\dagger}_{\mathrm{L}} g_{\mathrm{L}} \beta_{\mathrm{L}} \qquad \Sigma_{\mathrm{R}} = \beta_{\mathrm{R}} g_{\mathrm{R}} \beta^{\dagger}_{\mathrm{R}} \tag{5}$$

where g_{L} and g_{R} are the surface Green's functions of the left and right contacts, respectively, and β_{L} and β_{R} are the coupling

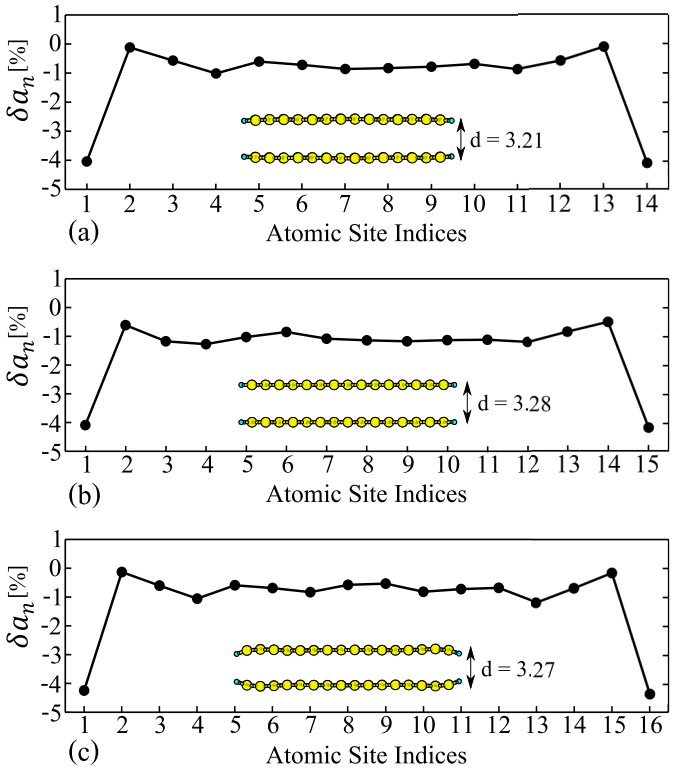

Fig. 2. Ratio of the C–C bonding length variation in the upper layer to the bonding length in an unrelaxed N_a-BLAGNR, i.e, $\delta a_n \equiv (a_n/1.422-1)\times 100$ [Fig. 1(a)], for (a) $N_a = 14$, (b) $N_a = 15$, and (c) $N_a = 16$. Inset: side view of the respective BLAGNR and its interlayer distance. Yellow and blue balls denote carbon and hydrogen atoms, respectively.

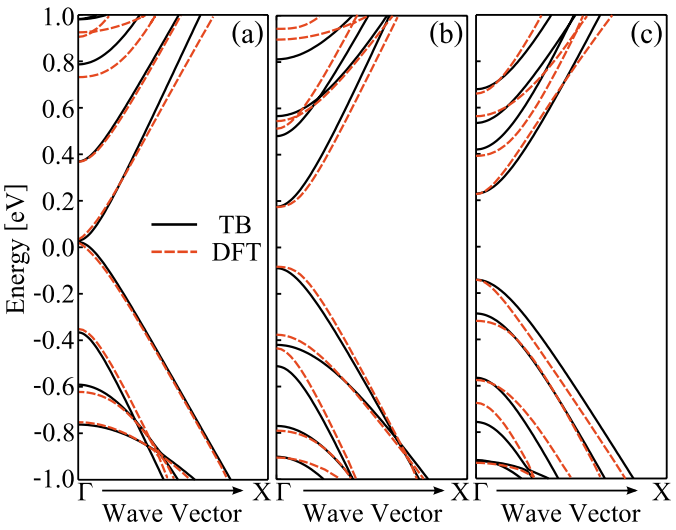

Fig. 3. TB and DFT calculated bandstructure of a relaxed N_a-BLAGNR for: (a) N_a=14, (b) N_a=15, and (c) N_a=16.

matrices between the device and the respective contact. The surface Green's functions can be efficiently calculated using the Sancho's iterative scheme [34]. The transmission probability of carriers in the device can be calculated using the following relation [35]:

$$T(E) = \text{Trace}[\Gamma_L G_{ch} \Gamma_R G_{ch}^{\dagger}] \tag{6}$$

where Γ is the broadening function and is defined as follows:

$$\Gamma_{L,R} = i[\Sigma_{L,R} - \Sigma_{L,R}^{\dagger}]. \tag{7}$$

Therefore, in the linear response regime the conductance of the device can be calculated as follows:

$$G(E) = -G_0 \int dE\ T(E) \left(\frac{\partial f}{\partial E}\right) \tag{8}$$

with $G_0 = 2e^2/h$. It is worth to mention that for 12-nm technology node, power supply voltage smaller than 0.7 V and equivalent oxide thickness of 0.59 nm is required. The latter corresponds to 3-nm-thick HfO_2 as the gate dielectric. A previous study showed that due to small values of quantum capacitance for GNRs, such a gate oxide can be neglected in the electrostatic design of BLAGNR-based FETs [40].

III. Results and Discussions

In the literature, a Poisson's ratio similar to that obtained experimentally for graphite is assumed whenever a graphene-based structure is considered [22], [36]. We have verified the validity of this assumption in the case of an AB-stacked BLG, within the elastic deformation regime. For this purpose, a full structural relaxation is performed until all the forces acting on atoms are smaller than 16 pN. Next, the uniaxial strain is applied to the relaxed structure. This is performed by stretching and compressing the unit cell along the x-direction to the desired value and tuning the lattice parameters in the y-direction; hence, the minimum of energy is reached. Therefore, we have calculated a Poisson's ratio equal to 16.50% for the AB-stacked BLG, by averaging the deformation percentages for the compressive and tensile cases. Noticeably, Poisson's ratio calculated confirms the previously adopted value.

Utilizing the standard convention in categorizing armchair GNRs, the notation N_a-BLAGNR refers to an armchair BLGNR with N_a dimer lines across its width, see Fig. 1(a). It was shown in previous studies that similar to SLAGNRs, BLAGNRs also exhibit three distinct families according to their electronic properties, following a modulo three periodic law, i.e., $N_a = 3p + k$, with p being an integer and $k = 0, 1, 2$ [20], [37]. To study the electronic properties of BLAGNRs under uniaxial strain, we have chosen nanoribbons with $N_a = 14$, 15, and 16 in our calculations to represent the three families. The dangling bonds located at the edges of BLAGNRs are assumed to be saturated with hydrogen atoms, which cause the carbon–carbon bonding lengths to be considerably different from those in the interior part of the structure. This phenomenon, known as edge bond relaxation, was previously studied in SLAGNRs and results in a 12% increase in hopping parameters for edge carbon atoms [38].

Fig. 2 shows the carbon–carbon bonding lengths parallel to the dimer lines in a 14-, 15-, and 16-BLAGNR. It can be seen that the interatomic distance between carbon atoms at the edges of the nanoribbon is reduced from 1.422 to 1.3626, 1.3619, and 1.3597 Åfor 14-, 15-, and 16-BLAGNR, respectively. The edge bonding lengths thus experience a 4%–4.25% reduction compared with the average C–C bonding lengths in

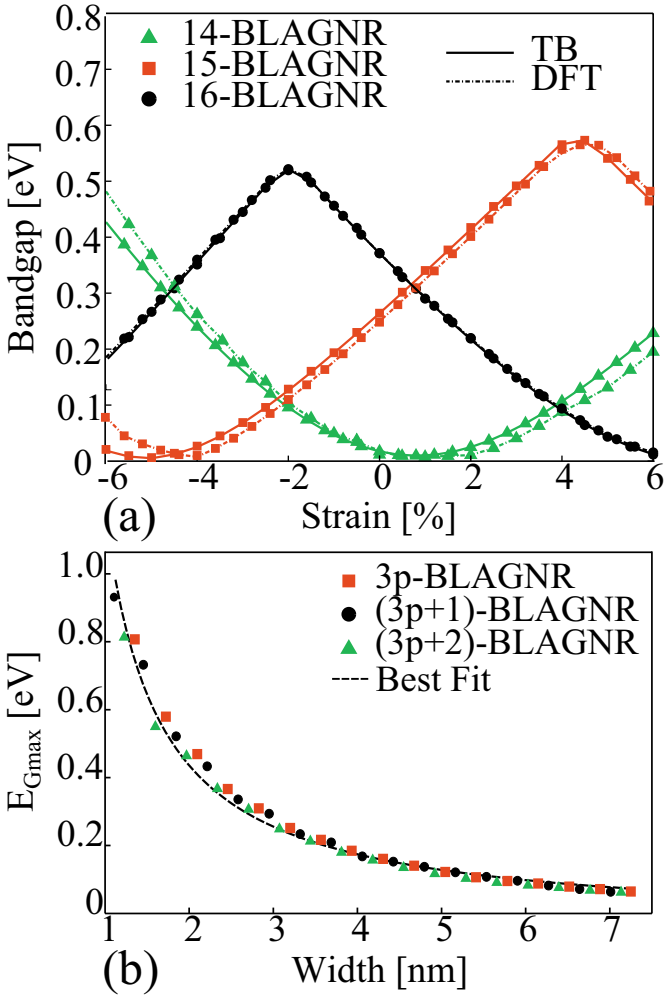

Fig. 4. (a) Variation of energy gap as a function of strain for 14-, 15-, and 16-BLAGNRs calculated from TB and DFT. (b) Maximum achievable bandgap as a function of the ribbon width for $3p$-, $(3p+1)$-, and $(3p+2)$-BLAGNRs, where p is an integer.

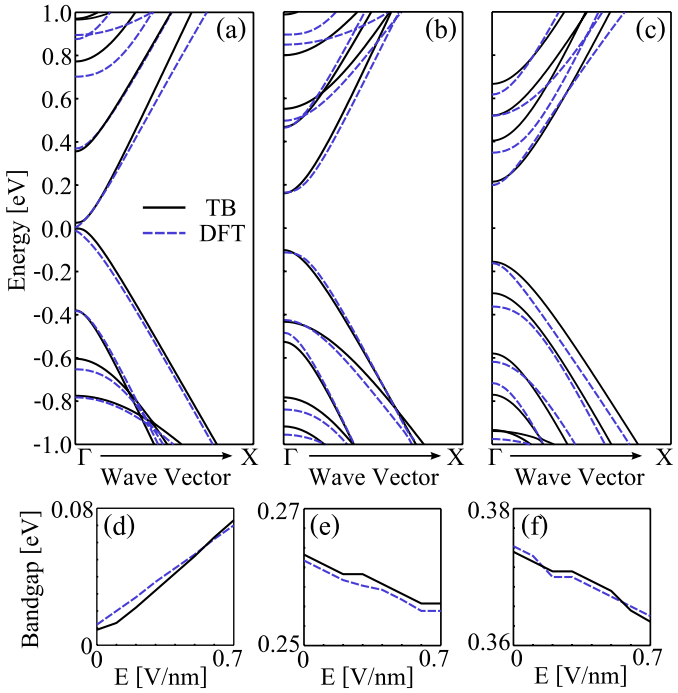

Fig. 5. (a)−(c) Bandstructures of 14-, 15-, and 16-BLAGNRs under E = 0.25V/nm calculated using DFT and TB methods. (d)−(f) Variation of bandgap for 14-, 15-, and 16-BLAGNRs with applied electric field employing both DFT and TB methods.

the inner parts. Therefore, according to (2), the increase in intralayer hopping parameter for the edge carbon atoms in the hydrogen-saturated case is predicted to be 7.3%–7.7%, which is smaller than that of their single layer counterparts. This difference can be due to the presence of interlayer interactions in BLAGNRs that further increase the charge density at the edges in comparison with SLAGNRs [37]. In addition, as shown in [37], different interlayer distances for various BLAGNRs was due to the difference in charge distribution at the edges.

Next, the electronic band structures for the undeformed BLAGNRs is calculated by employing both TB and DFT methods. The results are shown in Fig. 3(a)–(c) for 14-, 15-, and 16-BLAGNRs. The DFT calculations predict that these BLAGNRs have energy gaps of about 12, 261, and 369 meV, respectively, whereas TB calculations give 9, 265, and 372 meV, for these BLAGNRs. It is evident that the TB approximation with the consideration of edge bond effect is able to satisfactorily predict the bandgaps of relaxed nanoribbons. However, a closer look at the DFT and TB band structures of Fig. 3 shows that at higher energies there exist some discrepancies in the sub-band spacings between the DFT and TB results. It is later shown that these inconsistencies influence the strain dependence of the bandgap.

Another point worth noticing is that unlike the $(3p+2)$ subfamily of SLAGNRs, which are semiconductors with bandgaps in the range $\approx 0.05-0.3$ eV, the same subfamily of BLAGNRs exhibits a relatively small bandgap, in the range of 15–30 meV [37], [38]. A nanoribbon with such a small bandgap can be effectively considered as a metallic material at room temperature.

Fig. 4(a) compares the energy gaps of three subfamilies of BLAGNRs obtained from DFT and TB calculations. The magnitude of the applied strain is limited to $\pm 6\%$, to ensure that we are in the elastic regime where Poisson's ratio obtained for BLG is valid. It can be seen that similar to SLAGNRs, uniaxial strain strongly affects the bandgap of BLAGNRs. The dependency is in the form of sawtooth-shaped oscillations, i.e., the bandgap scales linearly with the magnitude of strain over a certain range, changes its slope at a turning point, and then this trend repeats as the strain is further increased. The linear dependence of energy gap on strain, however, is in the opposite direction for the subfamilies $3p$- and $(3p+1)$-BLAGNRs. In the subfamily $(3p+2)$-BLAGNR, the nanoribbon shows metal-semiconductor transition under all compressive strains and tensile strains larger than 2%. The high sensitivity of the energy gap to the applied strain in BLAGNRs renders them as suitable candidates for strain gauges. A similar phenomenon is utilized in carbon nanotube-based strain sensors [39].

In order for BLAGNRs to be applicable in strain sensors, their minimum and maximum attainable bandgaps should be

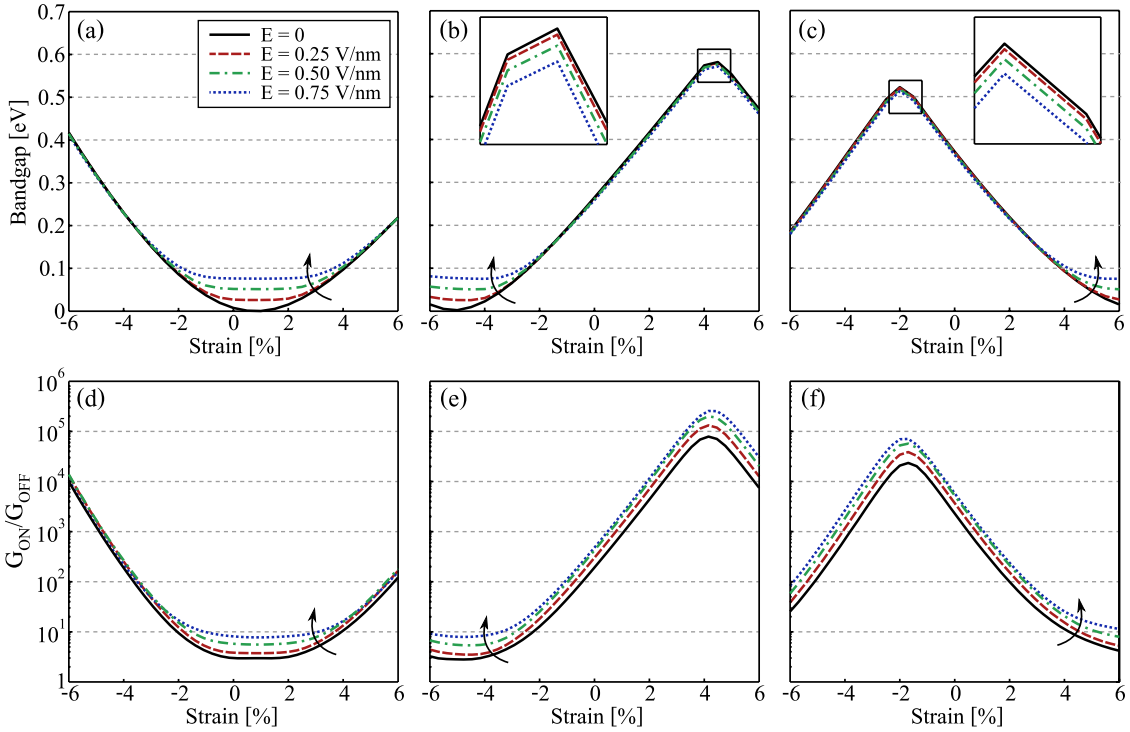

Fig. 6. (a)−(c) Strain dependence of the bandgap for 14-, 15-, and 16-BLAGNRs under various values of applied vertical electric field. (d)−(f) Variation of the on-off conductance ratio as a function of strain for 14-, 15-, and 16-BLAGNRs at 300 K. Arrows: increase of the amplitude of the applied electric field.

explored. Because of the semiconductor-metal transition the minimum achievable bandgap is equal to zero. The maximum predicted bandgap values are 0.48, 0.576, and 0.53 eV by DFT calculations and 0.43, 0.581, and 0.54 eV with TB method for 14-, 15-, and 16-BLAGNRs, respectively. Although there is a good agreement between the maximum bandgaps obtained from TB and DFT calculations, they do not occur at the same value of strain. As previously mentioned, this is due to the fact that sub-band spacing in TB and DFT calculated electronic bandstructures are not exactly similar at high energies; see Fig. 3. TB calculations for nanoribbons with different widths show that in general, the oscillation amplitude of bandgap decreases and the oscillations occur more frequently as the index of nanoribbon increases. As the oscillating behavior is due to the alternative movements of the sub-bands to the lower and higher energies with strain, such observation can be best explained by the relatively smaller sub-band spacings in wider nanoribbons. The maximum energy gap predicted by the TB model as a function of the ribbon's width is shown in Fig. 4(b). Apparently, the maximum energy gap is nearly subfamily independent especially for wider BLAGNRs. By fitting a curve to the results, one obtains a simple relation for the maximum achievable bandgap as a function of width: $E_{\mathrm{Gmax}} = 0.68/(W - 0.43)$, where E_{Gmax} is expressed in electron-volt and W is in nanometer. In addition, for ribbons with widths above 6 nm, E_{Gmax} is smaller than 0.1 eV. This implies that the application of uniaxial strain is not an effective method to induce the desired bandgap in BLG.

Fig. 5(a)−(c) shows the bandstructures of 14-, 15-, and 16- BLAGNRs under $E = 0.25\mathrm{V/nm}$. It can be seen that DFT and TB calculations predict very similar energy gaps and are quite identical especially at energies close to the bandgap. In Fig. 5(d)−(f), the variation of the bandgap with the applied electric field is shown for 14-, 15-, and 16-BLAGNRs, respectively. The results show that for 14-BLAGNR the bandgap increases with the applied electric field whereas for 15- and 16-BLAGNR the bandgap decreases with the increase of the electric field. Additionally, the ascending curve has a much steeper slope relative to the other two curves. These observations can be explained by referring to a previous study where a critical bandgap equal to 0.2 eV is calculated for BLAGNRs above which the bandgap decreases slowly with the electric field [20]. However, below this critical bandgap, increasing the electric field would significantly increase the bandgap as shown in Fig. 5(d). In addition, due to reduction of the bandgap with the ribbons width, the maximum attainable bandgap by applying a vertical electric field will be limited to that of BLG, which is 0.25 eV [17], [18].

Fig. 6(a)−(c) shows the variation of the bandgap versus strain under various values of applied vertical electric fields. As can be seen, the zigzag trend due to the application of strain is still dominant in the presence of the electric field. In addition, for energy gaps below 0.2 eV, raising the magnitude of the electric field increases the bandgap significantly while for energy gaps larger than 0.2 eV, increasing the electric field affects the bandgaps negligibly. Hence, the order of the curves for various electric fields are reversed below and above 0.2 eV.

Finally, to investigate the BLAGNR as a channel material to replace silicon in the critical 12-nm technology node [14], the ballistic on-off conductance ratio is evaluated for the projected supply voltage equal to 0.7 V. Hence, on and off state conductances are evaluated for $V_{\mathrm{GS}} = 0.7$ V and

$V_{GS} = 0$ V, respectively. Fig. 6(d)–(f) are the calculated on-off conductance ratio curves versus strain for 14-, 15-, and 16-BLAGNRs, respectively. Evidently, these curves follow an identical trend to that of the bandgap versus strain. Trying to explain this similarity, we inspected the curves for G_{ON} and G_{OFF}- the curves are not shown. Accordingly, G_{ON} follows the same trend as in the bandgap versus strain curves. However, G_{OFF} follows an opposite trend to that of G_{ON}. Therefore, the G_{ON}/G_{OFF} increases with the bandgap, reaching as high as 10^5, over satisfying the requirements for substituting silicon in the 12-nm technology node.

As the final remark, the AB-stacking BLAGNR studied in this paper [Fig. 1(a)] corresponds to the α-aligned bilayer armchair ribbons. The β-aligned ribbons, discussed in [20], with 50% larger bandgaps for the same width as their α-aligned counterparts, can be the subject of a future investigation.

IV. Conclusion

The effect of uniaxial strain and electric field on the electronic properties of BLAGNRs was investigated in this paper. Our DFT calculations indicated that by applying uniaxial strain to BLAGNRs, one can modulate the energy gaps in a periodic zigzag pattern. In addition, the effect of an applied vertical electric field on the energy gap was investigated. The results showed that by increasing the applied vertical electric field, the energy gap was decreased for BLAGNRs with zero electric field gaps below 0.2 eV and increased for those with zero electric field gaps above 0.2 eV.

To capture the edge bond relaxation effect, we showed that the TB parameters for edge carbon atoms should be increased by an average value of 7.3%–7.7% compared with that for the inner carbon atoms. The modified TB model resulted in energy gap trends identical to that predicted by DFT calculations for BLAGNRs subjected to uniaxial strain or external electric fields.

Additionally, the simultaneous effect of perpendicular electric field and uniaxial strain on the electronic bandgap was studied in this paper. The results showed the significant effect of the electric field on the bandgap, whenever the strain induced bandgap is smaller than a critical value of 0.2 eV.

Finally, our simulation results based on NEGF formalism revealed that for strained BLAGNRs, while the zigzag trend was preserved, an on-off conductance ratio as high as 10^5 can be achieved. Hence, by simultaneous application of strain and vertical electric field, BLAGNRs can be used as suitable substitutes to silicon as a channel material for FETs in the 12-nm technology node. In addition, the strong tunability of the bandgap of BLAGNRs with strain, make them promising candidates for electromechanical sensing applications, such as strain gauges.

Acknowledgment

The authors would like to thank H. Taghinejad and M. Taghinejad for their valuable discussions.

References

[1] K. Novoselov, A. Geim, and S. Morozov, D. Jiang, Y. Zhang, S. V. Dubonos, I. V. Grigorieva, and A. A. Firsov, "Electric field effect in atomically thin carbon films," *Science*, vol. 306, no. 5996, pp. 666–669, Oct. 2004.

[2] J. B. Oostinga, H. B. Heersche, X. Liu, A. F. Morpurgo, and L. M. K. Vandersypen, "Gate-induced insulating state in bilayer graphene devices," *Nature Mater.*, vol. 7, no. 2, pp. 151–157, Feb. 2008.

[3] Y. Zhang, T.-T. Tang, C. Girit, Z. Hao, M. C. Martin, A. Zettl, M. F. Crommie, Y. R. Shen, and F. Wang, "Direct observation of a widely tunable bandgap in bilayer graphene," *Nature*, vol. 459, no. 7248, pp. 820–823, Jun. 2009.

[4] T. Ohta, A. Bostwick, T. Seyller, K. Horn, and E. Rotenberg, "Controlling the electronic structure of bilayer graphene," *Science*, vol. 313, no. 5789, pp. 951–954, Aug. 2006.

[5] M. Y. Han, B. Ozyilmaz, Y. Zhang, and P. Kim, "Energy bandgap engineering of graphene nanoribbons," *Phys. Rev. Lett.*, vol. 98, no. 20, pp. 206805-1–206805-4, May 2007.

[6] Z. Chen, Y.-M. Lin, M. J. Rooks, and P. Avouris, "Graphene nanoribbon electronics," *Phys. E, Low-Dimensional Syst. Nanostruct.*, vol. 40, no. 2, pp. 228–232, Dec. 2007.

[7] X. Li, X. Wang, L. Zhang, S. Lee, and H. Dai, "Chemically derived, ultrasmooth graphene nanoribbon semiconductors," *Science*, vol. 319, no. 5867, pp. 1229–1232, Feb. 2008.

[8] L. Jiao, L. Zhang, X. Wang, G. Diankov, and H. Dai, "Narrow graphene nanoribbons from carbon nanotubes," *Nature*, vol. 458, no. 7240, pp. 877–880, Apr. 2009.

[9] L. Jiao, X. Wang, G. Diankov, H. Wang, and H. Dai, "Facile synthesis of high-quality graphene nanoribbons," *Nature Nanotechnol.*, vol. 6, no. 2, pp. 131–135, Jan. 2011.

[10] D. B. Shinde, J. Debgupta, A. Kushwaha, M. Aslam, and V. K. Pillai, "Electrochemical unzipping of multi-walled carbon nanotubes for facile synthesis of high-quality graphene nanoribbons," *J. Amer. Chem. Soc.*, vol. 133, no. 12, pp. 4168–4171, Mar. 2011.

[11] V. Pereira, A. H. C. Neto, and N. Peres, "Tight-binding approach to uniaxial strain in graphene," *Phys. Rev. B*, vol. 80, no. 4, pp. 1–8, Jul. 2009.

[12] Z. H. Ni, T. Yu, Y. H. Lu, Y. Y. Wang, Y. P. Feng, and Z. X. Shen, "Uniaxial strain on graphene: Raman spectroscopy study and band-gap opening," *Nano Lett.*, vol. 2, no. 11, pp. 2301–2305, Oct. 2008.

[13] C. Metzger, S. Rémi, M. Liu, S. V. Kusminskiy, A. H. C. Neto, A. K. Swan, and B. B. Goldberg, "Biaxial strain in graphene adhered to shallow depressions," *Nano Lett.*, vol. 10, no. 1, pp. 6–10, Jan. 2010.

[14] (2011). *International Technology Roadmap for Semiconductors (ITRS)* [Online]. Available: http:/www.itrs.net

[15] D. J. Frank, R. H. Dennard, E. Nowak, P. M. Solomon, and Y. Taur, "Device scaling limits of Si MOSFETs and their application dependencies," *Proc. IEEE*, vol. 89, no. 3, pp. 259–288, Mar. 2001.

[16] E. Castro, K. Novoselov, S. Morozov, N. Peres, J. D. Santos, J. Nilsson, F. Guinea, A. Geim, and A. H. Castro Neto, "Biased bilayer graphene: Semiconductor with a gap tunable by the electric field effect," *Phys. Rev. Lett.*, vol. 99, no. 21, pp. 216802-1–216802-4, Nov. 2007.

[17] P. Gava, M. Lazzeri, A. Saitta, and F. Mauri, "Ab initio study of gap opening and screening effects in gated bilayer graphene," *Phys. Rev. B*, vol. 79, no. 16, pp. 1–13, Apr. 2009.

[18] G. Fiori and G. Iannaccone, "On the possibility of tunable-gap bilayer graphene FET," *IEEE Electron Device Lett.*, vol. 30, no. 3, pp. 261–264, Mar. 2009.

[19] L. Jiao, X. Wang, G. Diankov, H. Wang, and H. Dai, "Facile synthesis of high-quality graphene nanoribbons," *Nature Nanotechnol.*, vol. 5, no. 5, pp. 321–325, May 2010.

[20] B. Sahu, H. Min, A. H. Macdonald, and S. K. Banerjee, "Energy gaps, magnetism, and electric field effects in bilayer graphene nanoribbons," *Phys. Rev. B*, vol. 18, no. 4, pp. 1–8, Jul. 2008.

[21] Y.-M. Lin and P. Avouris, "Strong suppression of electrical noise in bilayer graphene nanodevices," *Nano Lett.*, vol. 8, no. 8, pp. 2119–2125, Aug. 2008.

[22] Y. Lu and J. Guo, "Bandgap of strained graphene nanoribbons," *Nano Res.*, vol. 3, no. 3, pp. 189–199, May 2010.

[23] L. Sun, Q. Li, H. Ren, H. Su, Q. W. Shi, and J. Yang, "Strain effect on electronic structures of graphene nanoribbons: A first-principles study," *J. Chem. Phys.*, vol. 129, no. 7, pp. 074704-1–074704-6, Aug. 2008.

[24] O. Hod and G. E. Scuseria, "Electromechanical properties of suspended graphene nanoribbons," *Nano Lett.*, vol. 9, no. 7, pp. 2619–2622, Jul. 2009.

[25] G. Kresse and J. Furthmuller, "Efficient iterative schemes for ab-initio total-energy calculations using a plane-wave basis set," *Phys. Rev. B*, vol. 54, no. 16, pp. 11169–11186, Oct. 1996.
[26] G. Kresse and D. Joubert, "From ultrasoft pseudopotentials to the projector augmented-wave method," *Phys. Rev. B*, vol. 59, no. 3, pp. 1758–1775, 1999.
[27] P. E. Blöchl, "Projector augmented-wave method," *Phys. Rev. B*, vol. 50, no. 24, pp. 17953–17979, Dec. 1994.
[28] J. P. Perdew, K. Burke, and M. Ernzerhof, "Generalized gradient approximation made simple," *Phys. Rev. Lett.*, vol. 77, no. 18, pp. 3865–3868, Oct. 1996.
[29] J.-C. Charlier, J.-P. Michenaud, and X. Gonze, "First-principles study of the electronic properties of simple hexagonal graphite," *Phys. Rev. Lett.*, vol. 46, no. 8, pp. 4531–4539, Aug. 1992.
[30] H. Min, B. Sahu, S. Banerjee, and A. MacDonald, "*Ab initio* theory of gate induced gaps in graphene bilayers," *Phys. Rev. Lett.*, vol. 75, no. 15, pp. 155115-1–155115-7, Apr. 2007.
[31] T. B. Boykin, M. Luisier, N. Kharche, X. Jaing, S. K. Nayak, A. Martini, and G. Klimeck, "Multiband tight-binding model for strained and bilayer graphene from DFT calculations," in *Proc. 15th Int. Workshop Comput. Electron.*, May 2012, pp. 1–4.
[32] W. A. Harrison, *Electronic Structure and Properties of Solids*. New York, NY, USA: Dover, 1989.
[33] M. P. Anantram and A. Svizhenko, "Multidimensional modelling of nanotransistors," *IEEE Trans. Electron Devices*, vol. 54, no. 9, pp. 2100–2115, Sep. 2007.
[34] M. P. L. Sancho, J. M. L. Rubio, and L. Rubio, "Highly convergent schemes for the calculation of bulk and surface green functions," *J. Phys. F, Metal Phys.*, vol. 15, no. 4, pp. 851–858, Apr. 1985.
[35] Y. Meir and N. S. Wingreen, "Landauer formula for the current through an interacting electron region," *Phys. Rev. Lett.*, vol. 68, no. 16, pp. 2512–2515, Apr. 1992.
[36] O. L. Blakslee, D. G. Proctor, E. J. Seldin, G. B. Spence, and T. Weng, "Elastic constants of compression-annealed pyrolytic graphite," *J. Appl. Phys.*, vol. 41, no. 8, pp. 3373–3382, Aug. 1970.
[37] K.-T. Lam and G. Liang, "An ab-$initio$ study on energy gap of bilayer graphene nanoribbons with armchair edges," *Phys. Rev. Lett.*, vol. 92, no. 22, pp. 223106-1–223106-3, Jun. 2008.
[38] Y.-W. Son, M. L. Cohen, and S. G. Louie, "Energy gaps in graphene nanoribbons," *Phys. Rev. Lett.*, vol. 97, no. 21, pp. 1–4, Nov. 2006.
[39] J. Cao, Q. Wang, and H. Dai, "Electromechanical properties of metallic, quasimetallic, and semiconducting carbon nanotubes under stretching," *Phys. Rev. Lett.*, vol. 90, no. 15, pp. 157601-1–157601-4, Apr. 2003.
[40] T. Fang, A. Konar, H. Xing, and D. Jena, "Carrier statistics and quantum capacitance of graphene sheets and ribbons," *Phys. Rev. Lett.*, vol. 91, no. 9, pp. 092109-1–092109-3, Aug. 2007.

Authors' photographs and biographies not available at the time of publication.